Numerical Analysis of Turbulent Flow and Heat Transfer in a Square Sectioned U-Bend Duct by Elliptic-Blending Second Moment Closure

Jong-Keun Shin
Department of Automotive Engineering, Hanzhong University, 119 Jiheung-dong, Donghae, Kangwondo 240-713, Korea
Young-Don Choi*, Jeong-Soo An
Department of Mechanical Engineering, Korea University, 1 Anam-dong, Sungbuk-ku, Seoul 136-701, Korea

A second moment turbulence closure using the elliptic-blending equation is introduced to analyze the turbulence and heat transfer in a square sectioned U-bend duct flow. The turbulent heat flux model based on the elliptic concept satisfies the near-wall balance between viscous diffusion, viscous dissipation and temperature-pressure gradient correlation, and also has the characteristics of approaching its respective conventional high Reynolds number model far away from the wall. Also, the traditional GGDH heat flux model is compared with the present elliptic concept-based heat flux model. The turbulent heat flux models are closely linked to the elliptic-blending second moment closure which is used for the prediction of Reynolds stresses. The predicted results show their reasonable agreement with experimental data for a square sectioned U-bend duct flow field adopted in the present study.

Key Words : Second Moment Closure, Square Sectioned U-bend Duct Flow, Secondary Flow, Elliptic-Blending Model, Turbulent Heat Transfer

1. Introduction

Turbulent flow and heat transfer through the passage of turbine blades and heat exchangers are examples of turbulent duct flows with strong streamline curvature and secondary flow. The pressure induced by secondary flow motions produces significant outcomes in the turbulent duct flows and thus, affects the level of heat transfer (Suga, 2003). To investigate this kind of turbulent duct flow, Chang et al.(1983) provided the detailed structure of the turbulence in a square sectioned U-bend duct by experiments. Also, the heat transfer characteristics related to the local Nusselt number and temperature distributions in the same geometry were measured by Johnson (1984) and Johnson & Launder (1985). These studies detected a trough in the streamwise mean velocity profiles and indicated that unprecedented velocity distributions originated from strong secondary flow motions.

The characteristics of turbulence and heat transfer in square sectioned U-bend duct flows were predicted by many numerical studies. In the survey carried out by Iacovides and Launder (1995), who obtained good numerical results, a low Reynolds number (LRN) model was found to be for more reliable than wall functions. They also recommend the use of a second moment closure to predict duct flows despite the problems of the wall-reflection terms in modeling the pres-

* Corresponding Author,
E-mail : ydchoi@korea.ac.kr
TEL : +82-2-3290-3355; **FAX** : +82-2-928-1067
Department of Mechanical Engineering, Korea University, 1 Anam-dong, Sungbuk-ku, Seoul 136-701, Korea.
(Manuscript **Received** September 4, 2006; **Revised** December 4, 2006)

sure-strain correlation (Suga, 2003).

Although solving every component of Reynolds stress transport equations requires more computational resources than adopting an eddy viscosity model, second moment closures are considered to be more general closure. To obtain the numerical computations of flow characteristics in detail, several more advanced LRN second moment closures were applied to the square sectioned U-bend duct flow and the results of the predictions were in good agreement with the experimental data. Among them, the model proposed by Craft & Launder (1996) was considered to be thoroughly free from the topographical parameters such as wall-normal distance and wall normal vector. For industrial applications, dropping these parameters is much preferred because of the complexity of the flow geometry (Suga, 2003).

Although the more advanced LRN second moment closures are well established based on a sound theory, the near-wall models for pressure-strain correlation or pressure diffusion term possesses so complicated forms. This fact means that the possibility of numerical stiffness is always existed in the models. From these reasons, the LRN second moment closures have not been loaded easily on any commercial code and they are not widely used in industrial applications.

On the other hand, for the turbulent stress field, Durbin (1993) introduced the elliptic relaxation method (ERM), which uses a new type of wall blocking model. The method, applied to Reynolds stress models, has a solid theoretical basis, but implies six additional equations, so it is not widely used in the industry. The complex implementation and the stability problems of this method are the main problems, and the boundary conditions for the additional equations are a major source of numerical instability (Manceau & Hanjalic, 2002). To overcome the weak points of the ERM, Thielen et al.(2004) suggested another approach, called "the elliptic-blending model (EBM)", which is based on a blending of near-wall and far-from the wall forms of pressure scrambling correlation. The ellipticity is preserved by solving an elliptic-blending function. The model guarantees the main feature of the Durbin's elliptic relaxation second moment model but involves only one scalar elliptic equation, applying a simple boundary condition at the wall. Also, the model can be used in the industry because it offers a reasonable compromise between simplicity and consistency of physics. A notable feature of these approaches is that the non-local character on pressure scrambling term is preserved by the elliptic operators such as the elliptic relaxation equation or the elliptic-blending equation, and the formulations can be integrated down to the wall (Manceau & Hanjalic, 2002).

In the heat transfer calculations, the generalized gradient diffusion hypothesis (GGDH) of Daly & Harlow (1970) is usually applied to predict the turbulent heat flux in combination with second moment closures. Although the GGDH model is adopted in a non-linear eddy viscosity model, since the GGDH heat flux model mainly relies on the predicted turbulence anisotropy, it is reasonably expected that coupling it with a second moment closure is more suitable for predicting complex thermal fields (Suga, 2003). GGDH can not predict the streamwise heat flux component reasonably well (Launder, 1988). Although the streamwise component is not important for predicting the thermal field in a fully developed flow parallel to the wall, it does not necessarily mean that the streamwise component is always unimportant. Therefore, to improve the information for the characteristics of turbulent heat transfer in curved ducts, the other proposals for turbulent heat flux model, which has better accuracy in predicting the streamwise component, should be adopted in square sectioned U-bend duct flow with heat transfer. Unlike the gradient diffusion model form, the elliptic concept turbulent heat flux model proposed by Shin et al.(2005), among the improved models, solves the turbulent heat flux transport equation. And, the model satisfies the near-wall balance between viscous diffusion, viscous dissipation and temperature-pressure gradient correlation, and can also approach its respective conventional high Reynolds number model far away from the wall.

Thus, the present study uses the elliptic concept heat flux model, which is closely associated with

the EBM of Thielen et al., considering the possibility of its use in the industry, and the prediction results are compared with those of GGDH model predictions and experimental data of Johnson (1984) and Johnson & Launder (1985).

2. Mathmatical Models

2.1 Elliptic-blending model for the turbulent stress tensor

The model transport equation for the turbulent stress tensor, which constitutes the elliptic-blending second moment closure (Thielen et al., 2004), can be given as follows:

$$\frac{D\overline{u_iu_j}}{Dt}=\frac{\partial}{\partial x_k}\left(v\delta_{kl}\frac{\partial\overline{u_iu_j}}{\partial x_l}\right)+D_{ij}^T+P_{ij}+\Phi_{ij}^*-\varepsilon_{ij} \quad (1)$$

where P_{ij} and ε_{ij} are identified as the stress production and dissipation rate, respectively, with $P=1/2P_{kk}$ and $\varepsilon=1/2\varepsilon_{ii}$, and Φ_{ij}^* is the velocity- pressure gradient correlation, known as the pressure scrambling term.

To impose a limitation on the fluctuating quantities of Reynolds stresses, Durbin (1993) proposed the ERM as

$$\Phi_{ij}^*-\varepsilon_{ij}=kf_{ij}=\frac{\overline{u_iu_j}}{k}\varepsilon \quad (2)$$

In equation (2), f_{ij} is obtained from the elliptic relaxation equation as

$$f_{ij}-L^2\nabla^2f_{ij}=\frac{1}{k}\left(\Phi_{ij}^h-\frac{2}{3}\varepsilon\delta_{ij}+\frac{\overline{u_iu_j}}{k}\varepsilon\right) \quad (3)$$

Also, Durbin (1993) suggested the wall boundary conditions of f_{ij} equations to reproduce the wall-limiting behavior of $\Phi_{ij}^*-\varepsilon_{ij}$. However, because the six additional equations for f_{ij} induce the numerical stiffness by the imposed boundary conditions, Thielen at al.(2004) proposed a simpler model preserving the main features of the ERM; this model is called the elliptic-blending method (herein after EBM), which blends the "homogeneous" (away-from-the-wall) and near-wall models of Φ_{ij}^* and ε_{ij} as follows:

$$\Phi_{ij}^*=(1-\psi^2)\,\Phi_{ij}^w+\psi^2\Phi_{ij}^h \quad (4)$$

$$\varepsilon_{ij}=(1-\psi^2)\frac{\overline{u_ik_j}}{k}\varepsilon+\psi^2\frac{2}{3}\varepsilon\delta_{ij} \quad (5)$$

where ψ is an elliptic-blending parameter, obtained by solving an elliptic differential equation

$$\psi-L^2\nabla^2\psi=1, \quad (6)$$

with the boundary conditions $\psi=0$ at the wall. For the reproduction of the wall-limiting behavior of Φ_{ij}^w, Thielen et al.(2004) suggested the near-wall redistribution term.

$$\Phi_{ij}^w=-5\frac{\varepsilon}{k}\left(\overline{u_iu_k}n_jn_k+\overline{u_ju_k}n_in_k-\frac{1}{2}\overline{u_ku_l}n_kn_l(n_in_j+\delta_{ij})\right), \quad (7)$$

where the unit wall-normal vector is evaluated from

$$\mathrm{n}=\frac{\nabla\psi}{\|\nabla\psi\|}. \quad (8)$$

Concerning the quasi-homogeneous model Φ_{ij}^h $(=\Phi_{ij}^{slow}+\Phi_{ij}^{rapid})$, Thielen et al.(2004) adopted the following model of Speziale et al.(1991).

$$\begin{aligned}\Phi_{ij}^h=&-\left(C_1+C_1^*\frac{P}{\varepsilon}\right)\varepsilon b_{ij}\\&+C_2\left(b_{ik}b_{kj}-\frac{1}{3}b_{kl}b_{kl}\delta_{ij}\right)\\&+(C_3-C_3^*\sqrt{b_{kl}b_{kl}})\,kS_{ij}\\&+C_4k\left(b_{ik}S_{jk}+b_{jk}S_{ik}-\frac{2}{3}b_{lm}S_{lm}\delta_{ij}\right)\\&+C_5k(b_{ik}W_{jk}+b_{jk}W_{ik})\end{aligned} \quad (9)$$

where

$$b_{ij}=\frac{\overline{u_iu_j}}{2k}-\frac{1}{3}\delta_{ij} \quad (10)$$

is the anisotropy tensor. Also, in equation (9)

$$S_{ij}=\frac{1}{2}\left(\frac{\partial U_i}{\partial x_j}+\frac{\partial U_j}{\partial x_i}\right);\qquad W_{ij}=\frac{1}{2}\left(\frac{\partial U_i}{\partial x_j}-\frac{\partial U_j}{\partial x_i}\right) \quad (11)$$

represent the mean rate of strain and the mean vorticity tensor, respectively.

The unclosed diffusion term in equation (1) is modeled by gradient diffusion as

$$D_{ij}^T=\frac{\partial}{\partial x_k}\left(C_s\overline{u_ku_l}T\frac{\partial\overline{u_iu_j}}{\partial x_l}\right) \quad (12)$$

with the coefficient $C_s=0.21$.

Accordingly, substituting equations (4), (5)

and (12) into equation (1), we can obtain the Reynolds stress equation model based on EBM, and the model equations should be converted into the cylindrical coordinate. The model transport equation for the energy dissipation rate can be given in cylindrical coordinates as follows:

$$\begin{aligned}&\frac{\partial}{\partial x}(\rho U\varepsilon)+\frac{1}{r}\frac{\partial}{\partial r}(rpV\varepsilon)+\frac{\partial}{r\partial\theta}(\rho W\varepsilon)\\&=\frac{\partial}{\partial x}\left[(\mu+\rho C_\varepsilon T\overline{u^2})\frac{\partial\varepsilon}{\partial x}\right]\\&\quad+\frac{1}{r}\frac{\partial}{\partial r}\left[r(\mu+\rho C_\varepsilon T\overline{v^2})\frac{\partial\varepsilon}{\partial r}\right]\\&\quad+\frac{\partial}{\partial x}\left[\rho C_\varepsilon T\left(\overline{uv}\frac{\partial\varepsilon}{\partial r}+\overline{uw}\frac{\partial\varepsilon}{r\partial\theta}\right)\right]\\&\quad+\frac{1}{r}\frac{\partial}{\partial r}\left[r\rho C_\varepsilon T\left(\overline{uv}\frac{\partial\varepsilon}{\partial x}+\overline{vw}\frac{\partial\varepsilon}{r\partial\theta}\right)\right]\\&\quad+\frac{\partial}{r\partial\theta}\left[r\rho C_\varepsilon T\left(\overline{uw}\frac{\partial\varepsilon}{\partial x}+\overline{vw}\frac{\partial\varepsilon}{\partial r}\right)\right]\\&\quad+\frac{\rho(C_{\varepsilon1}P-C_{\varepsilon2}\varepsilon)}{T}\end{aligned}\tag{13}$$

where,

$$\begin{aligned}P=-\rho&\left[\overline{u^2}\frac{\partial U}{\partial x}+\overline{uv}\left(\frac{\partial V}{\partial x}+\frac{\partial U}{\partial r}\right)+\overline{uw}\left(\frac{\partial W}{\partial x}+\frac{\partial U}{r\partial\theta}\right)\right]\\&+\overline{v^2}\frac{\partial V}{\partial r}+\overline{vw}\left(\frac{\partial W}{\partial r}+\frac{\partial V}{r\partial\theta}-\frac{W}{r}\right)+\overline{w^2}\left(\frac{\partial W}{r\partial\theta}+\frac{V}{r}\right)\end{aligned}\tag{14}$$

is production of the turbulent kinetic energy, and the model coefficient $C_{\varepsilon1}$ is assigned as

$$C_{\varepsilon1}=1.44\left(1+0.03(1-\psi^2)\sqrt{\frac{k}{u_iu_jn_in_j}}\right).\tag{15}$$

The other coefficients appearing in the equation are $C_{\varepsilon2}=1.83$ and $C_\varepsilon=0.18$.

In the above equations, the turbulent time scale T and length scale L are bounded by Kolmogorov scales as were in the elliptic relaxation method of Durbin (1993):

$$T=\max\left(\frac{k}{\varepsilon},\ C_T\left(\frac{\nu}{\varepsilon}\right)^{1/2}\right)\tag{16}$$

$$L=C_L\max\left(\frac{k^{3/2}}{\varepsilon},\ C_\eta\frac{\nu^{3/4}}{\varepsilon^{1/4}}\right)\tag{17}$$

The model coefficients adopted in the present study is listed in Table 1.

Table 1 The model coefficients for Thielen et al.'s EBM

C_1	C_1^*	C_2	C_3	C_3^*	C_4	C_5	C_T	C_L	C_η
3.4	1.8	0	0.8	1.3	1.25	0.4	6.0	0.161	80.0

2.2 Turbulent heat flux model using the elliptic-blending equation

A mathematical model of turbulent scalar transport is required to solve the Reynolds-averaged scalar equation. In the second moment closure, the generation term due to mean velocity and scalar gradients can be handled exactly, and this feature should be one of the most attractive advantages for the prediction of complex flows. The transport equations for mean temperature and scalar flux in a fluid of constant physical properties are given as:

$$\frac{D\Theta}{Dt}=\frac{\partial}{\partial x_{ij}}\left(\alpha\frac{\partial\Theta}{\partial x_j}-\overline{u_j\theta}\right)\tag{18}$$

$$\frac{D\overline{u_i\theta}}{Dt}=P_{i\theta}+D_{i\theta}^T+D_{i\theta}^v+\Phi_{i\theta}^*-\varepsilon_{i\theta}\tag{19}$$

In equation (19), $P_{i\theta}$ denote production by temperature and velocity gradients, which is exactly expressed as

$$P_{i\theta}=-\overline{u_iu_k}\frac{\partial\Theta}{\partial x_k}-\overline{u_k\theta}\frac{\partial U_i}{\partial x_k},\tag{20}$$

and $D_{i\theta}^T$, $D_{i\theta}^v$, $\Phi_{i\theta}^*$ and $\varepsilon_{i\theta}$ are unclosed terms and mean turbulent diffusive transport, viscous diffusive transport, pressure scrambling (temperature-pressure gradient correlation) and molecular dissipation of heat fluxes, respectively.

For the modeling of the unclosed terms in equation (19), the near-wall behaviour of the heat flux equations must be considered. Satisfying the limiting behaviour of the models at the wall is one of the basic requirements of near-wall modeling. In order to adopt the elliptic-blending concept turbulent heat flux model, the model of Shin et al.(2005) is employed in this study.

Firstly, the turbulent diffusion term in equation (19) is modeled based on the standard gradient transport hypothesis as:

$$D_{i\theta}^t=\frac{\partial}{\partial x_k}\left(C_\theta\overline{u_ku_l}T\frac{\partial\overline{u_i\theta}}{\partial x_l}\right)\tag{21}$$

with an adjustable coefficient C_θ.

Unlike the Reynolds stress model, the molecular diffusion is not of the correct term. The model suggested by Lai & So (1990) is adopted for the wall limiting condition as:

$$D_{i\theta}^{v}=v\frac{\partial^2\overline{u_i\theta}}{\partial x_k^2}+\frac{\alpha-v}{n_i+2}\frac{\partial^2\overline{u_i\theta}}{\partial x_k^2} \quad (\text{no summation for } i) \tag{22}$$

In equation (22), the n_i means the unit normal to the wall.

The temperature-pressure gradient correlation term $\Phi_{i\theta}^{*}$ and the dissipation term $\varepsilon_{i\theta}$ are the major sink terms and need to be carefully modeled. By following the same approach as that for the turbulent stress field, Shin et al. (2005) expressed the pressure scrambling with the elliptic-blending equation analogue to Thielen et al.'s EBM as:

$$\Phi_{i\theta}^{*}=(1-\psi^2)\,\Phi_{i\theta}^{w}+\psi^2\Phi_{i\theta}^{h} \tag{23}$$

In the above model, the ellipticity of the model is preserved by solving elliptic differential equation (6). For $\Phi_{i\theta}^{h}$, any known quasi-homogeneous model can be adopted, and the general linear model (Durbin, 1993) is chosen in the present study as:

$$\Phi_{i\theta}^{h}=-C_{1\theta}\frac{\varepsilon}{k}\overline{u_i\theta}+C_{2\theta}\overline{u_j\theta}\frac{\partial U_i}{\partial x_j}+C_{3\theta}\overline{u_iu_j}\frac{\partial\Theta}{\partial x_j} \tag{24}$$

with adjustable coefficients. Because the molecular destruction at high Reynolds number flows is significant only in the vicinity of a solid wall, an expression satisfying the above constraints together with $\Phi_{i\theta}^{*}$ can be proposed as:

$$\varepsilon_{i\theta}=\frac{1}{2}\left(1+\frac{1}{\mathrm{Pr}}\right)\frac{\varepsilon}{k}\overline{u_i\theta} \tag{25}$$

To impose the limiting wall behaviour of turbulent heat fluxes, $\Phi_{i\theta}^{w}$ can be modeled such that it will approach its asymptotic value near the wall.

$$\Phi_{i\theta}^{w}=-\left[1+\frac{1}{2}\left(1+\frac{1}{\mathrm{Pr}}\right)\right]\frac{\varepsilon}{k}\overline{u_k\theta}n_kn_i. \tag{26}$$

From the combination of equations (25) and (26), we know that the limiting wall behaviour of $\Phi_{i\theta}^{w}-\varepsilon_{i\theta}$ is artificially satisfied. For the reproduction of the limiting wall behaviour of $\Phi_{i\theta}^{w}$, the unit wall-normal vector is used. However, the use of a wall-normal vector must be avoided, since such a quantity is often not well defined in complex geometries. Therefore, in the present work, a new formulation (8) suggested by Thielen et al. (2004) is also adopted.

The model coefficients for Shin et al.'s elliptic-blending heat flux model (herein after EBHM) are listed in Table 2.

Table 2 The model coefficients for EBHM

C_θ	$C_{1\theta}$	$C_{2\theta}$	$C_{3\theta}$
0.153	3.0	0.4	0.25

2.3 GGDH model

In equation (18), turbulent heat flux $\overline{u_i\theta}$ can be obtained by a simple model, not through the transport equations used in EBHM. The popular GGDH (generalized gradient diffusion hypothesis) model of Daly and Harlow (1970) is expressed as

$$\overline{u_i\theta}=-C_{\theta\theta}T\overline{u_iu_j}\frac{\partial\Theta}{\partial x_j}. \tag{27}$$

The GGDH model can be adopted successfully in complex turbulent heat transfer computations when near-wall turbulence anisotropy is well reproduced (Launder, 1988). Thus, since a GGDH heat flux model mainly relies on the predicted turbulence anisotropy, it is expected that coupling it with a second moment closure is more suitable than any eddy viscosity model for predicting complex thermal fields (Suga, 2003). GGDH can not correctly predict the streamwise heat flux component in a fully developed flow parallel to the wall. To improve the performance of the GGDH model, an expanded version of the GGDH model was suggested by Suga & Abe (2000).

When the turbulence anisotropy in near-wall of the square sectioned U-bend duct flow is reasonably well reproduced by the Thielen et al's EBM, we will investigate whether or not the GGDH model can capture the characteristics of turbulent heat transfer. The model coefficient $C_{\theta\theta}$ in equation (27) is set to 0.3.

3. Numerical Treatment

Figure 1 shows the flow geometry with a bend radius equal to 3.375 times the hydraulic diameter of the duct. The flow Reynolds number based on the hydraulic diameter was 56690. The streamwise velocity component was set to W and cross-sectional velocities U and V respectively. The flow configuration presently employed was the same as that in a previous study (Johnson, 1984). The equations of mean motion for the turbulent flow around a square sectioned U-bend duct were conveniently expressed in cylindrical coordinates. A fine grid employed to cover the half cross-section of the duct between the symmetry plane and on each wall was 52×100 in the normal and radial directions, respectively. The first near wall point inside the domain was located at $y^+=0.5$ to capture the limiting wall behaviour of Reynolds stresses. In the bend section, 116 planes were used and additional 20 planes were employed for the inlet and exit tangents extending 10 hydraulic diameters upstream and downstream, respectively. The non-diffusive QUICK approximation was used for discretizing the convective transport in the cross-sectional plane of the duct.

The inlet conditions at the beginning of the computational domain were taken from the experimental data of Melling & Whitelaw (1976). The distribution of the inlet temperature distributions was derived from the experimental data acquired by Johnson (1984). The constant wall heat flux condition at the each wall was given for the thermal field computation. The boundary conditions specified at the computational domain are summarized as ;

Wall : $u_i=\overline{u_iu_j}=\overline{u_i\theta}=0,$
$\varepsilon=2\nu(\partial\sqrt{k}/\partial y)^2,\ \psi=0$

Symmetry plane :
$U=\overline{uv}=\overline{uw}=\overline{u\theta}=0,$
$\dfrac{\partial\phi}{\partial x}=0\ (\phi=V, W, \varepsilon, \overline{u_iu_i}, \overline{vw}, \psi, \overline{v\theta}, \overline{w\theta})$

Outlet : $\dfrac{\partial\phi}{\partial z}=0\ (\phi=U_i, \varepsilon, \overline{u_iu_j}, \Theta, \overline{u_i\theta})$

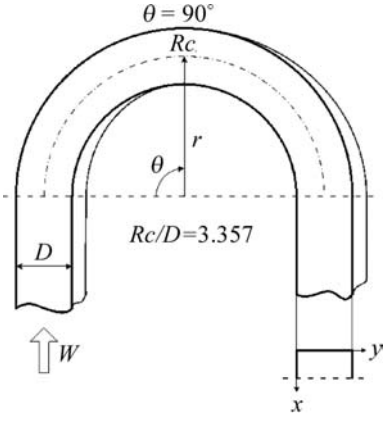

Fig. 1 Square sectioned 180° U-bend duct

4. Results and Discussion

Figure 2 compares the predicted streamwise mean velocity distributions at sections $\theta=45°$, 90°, 135° and 180°, respectively. At each section,

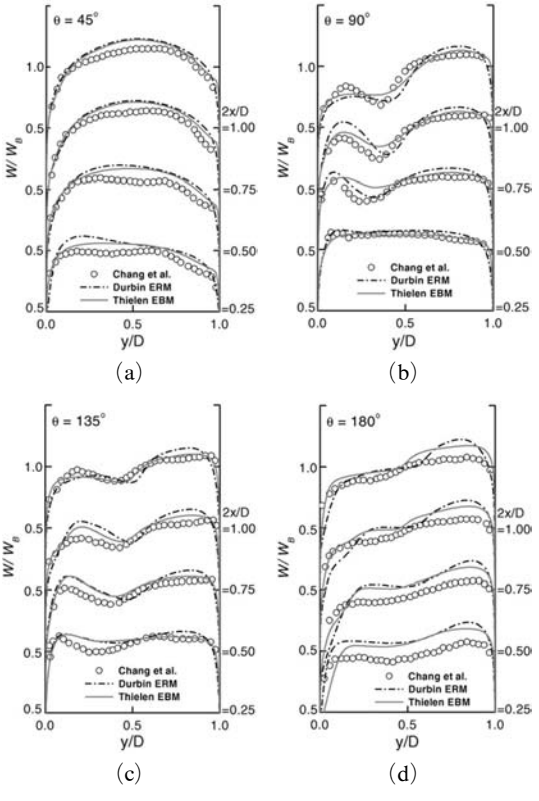

Fig. 2 Streamwise mean velocity profiles in the U-bend duct at Re=56690

the velocity distribution at $2x/D=0.25$, 0.5, 0.75 and 1.0 is reproduced. The current primary flow was obtained from the prediction of the strong secondary motion, which give rise to the trough in the streamwise velocity near the inside of the bend. The ability of velocity profile prediction by the present EBM was compared with that of the ERM of Durbin (1993) and the experiments of Chang et al.(1983). Although there was no perfect agreement between the predictions and experiments, both elliptic concept models generally reproduced well the characteristic of streamwise velocity. Figure 2(a) shows that, at $\theta=45°$ of the bend, the models gave very similar prediction results with the measured velocity profiles. As shown in Fig. 2(b) and 2(c), the main characteristic of this flow was the appearance of the trough shapes in the streamwise velocity distribution. These shapes were the results of the loss of streamwise momentum due to the cross-sectional strong secondary flow. The shape of troughs near the inside ($y/D=0$) of the bend at $\theta=90°$ and 135° was better predicted by ERM than EBM. However, in the outer ($y/D=1$) region of the bend, the results by EBM were considerably in better agreement with the measured data than those by ERM were. The results of EBM and the measured data were in particularly good agreement at $\theta=135°$.

Figures 3(a) and 3(b) show the distributions of rms streamwise turbulent velocity w_{rms} and shear stress $\overline{uw}$ at $\theta=90°$. While the ERM yields good predictions on the shape of w_{rms} distribution, the EBM is closer to the experimental data in the accuracy of the evaluated values. Especially, $\overline{vw}/W_B$ profiles due to the EBM exhibit distributions similar to the experimental data.

Figure 4 shows the distributions of non-dimensional temperature $\Theta^+(=(T-T_W)/(T_B-T_W))$ at the cross section of $\theta=45°, 90°, 135°$ and 180°. T_W is the wall temperature at $2x/D=1.0$ of the outer wall and T_B is the bulk temperature. That is, predictions by both the EBHM and the GGDH model combined with the EBM are plotted against the experimental results of Johnson (1984). With respect to the prediction of Θ^+ distribution in the U-bend duct, as mentioned, the flow field reproduced by the EBM is employed in the turbulent heat transfer computation. As a whole, the prediction due to EBHM is similar to that of the GGDH model. This result means that the EBHM does not greatly affect the thermal field prediction

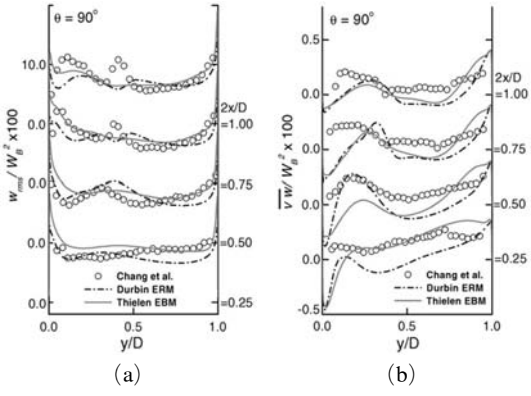

Fig. 3 Reynolds stresses in the U-bend duct at $\theta=90°$

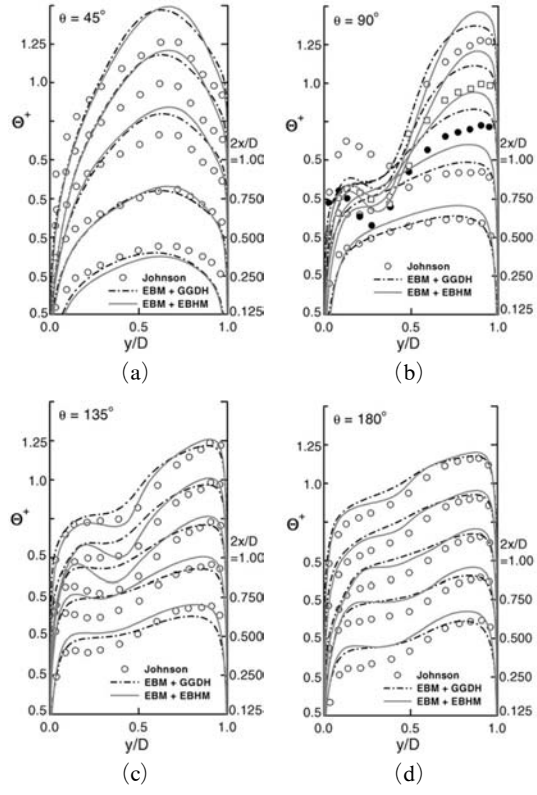

Fig. 4 Non-dimensional temperature profiles in the U-bend duct at Re=56690 and Pr=0.71

in the U-bend duct. However, it can be shown that the prediction of GGDH model is closer to the experiment results up to $\theta=90°$ in the U-bend, while the EBHM reproduces better results and shape than the GGDH model does, beyond $\theta=135°$ in U-bend. At $\theta=45°$ the non-dimensional temperature profiles near the outer wall $(y/D=1.0)$ are considerably higher than those near the opposite wall, with the peak displaced towards the outer wall.

Although some discrepancies are observed in the regions of $2x/D\geq 0.75$, the predictions show good distributions when compared to the experiments. A difference pattern emerges at $\theta=90°$, where the minimums in the non-dimensional temperature mimic the trough in the streamwise velocity profile for $2x/D=0.5$, 0.75 and 1.0. Despite of relatively correct prediction for the streamwise velocity, the non-dimensional temperature distributions by the models deviated from those of the experiments in regions of $2x/D>0.5$. This is due to the incorrect prediction of the levels of turbulent velocity fluctuations in these regions. However, the predictions by the EBHM at $\theta=135°$ and 180° show good reproduction for the shape and magnitude in comparison with experiments.

In Fig. 5, the predicted local Nusselt number Nu distributions at the sections of $\theta=0°$, 45°, 90°, 135° and 180° are compared with the experimental data of Johnson & Launder (1985).

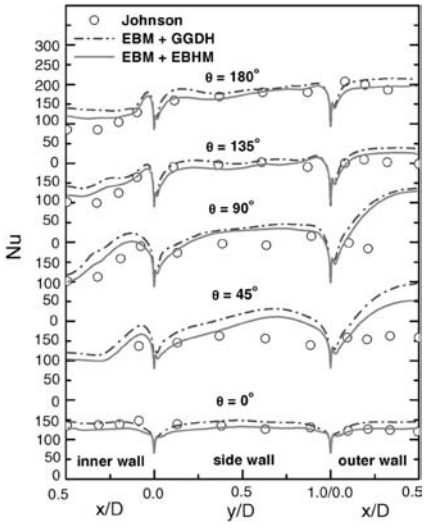

Fig. 5 Local Nusselt number distributions in the U-bend duct flow at Re=56690 and Pr=0.71

The level of agreement between the models and experiments were fairly reasonable though some discrepancies can be found at $\theta=45°$ and 90° of the outer wall. The high level local Nusselt number distributions at $\theta=45°$ and 90° were the consequence of the over-prediction of the non-dimensional temperature profiles in outer wall region which were obvious in Figs. 4(a) and 4(b). The prediction based on the EBHM was slightly better than that of GGDH.

Figure 6 shows the prediction patterns of the streamwise velocity contour and the secondary flow vector in the left-hand-side of the U-bend duct cross section by EBM of Thielen et al., and the non-dimensional temperature contour by EBHM in the right-hand-side of the cross section. From the secondary flow patterns, we can infer the sequence of developments that give rise to the trough in the profile of the streamwise velocity near the inside of the bend. Over the initial part of the bend, the conventional single secondary flow carries the near-wall fluid to the inside $(y/D=0)$ of the bend. Due to this accumulation, slow moving fluid near the symmetry plane is pushed away from the inside wall towards the outside $(y/D=1)$ of the bend. However, because its streamwise velocity is low, it cannot proceed against the radial pressure gradient. Thus, the interaction of primary and secondary flows leads to a progressive vortex breakdown. The streamwise velocity contours shown in Fig. 6 are distorted in an obvious way by this secondary flow pattern, and this distortion leads to the appearance of the trough in the profiles of Fig. 2. From the predicted thermal field contours, also, we can see that the non-dimensional temperature distribution is strongly affected by the steamwise velocity, especially beyond $\theta=135°$ of the bend. That is, the non-dimensional temperature contour patterns are very similar to the streamwise mean velocity contours with the exception at $\theta=90°$. Like the contour of the streamwise velocity, the contour of non-dimensional temperature corresponding to $\theta=180°$ is, stratified in the outer wall region $(y/D=1)$ of the cross-section, indicating

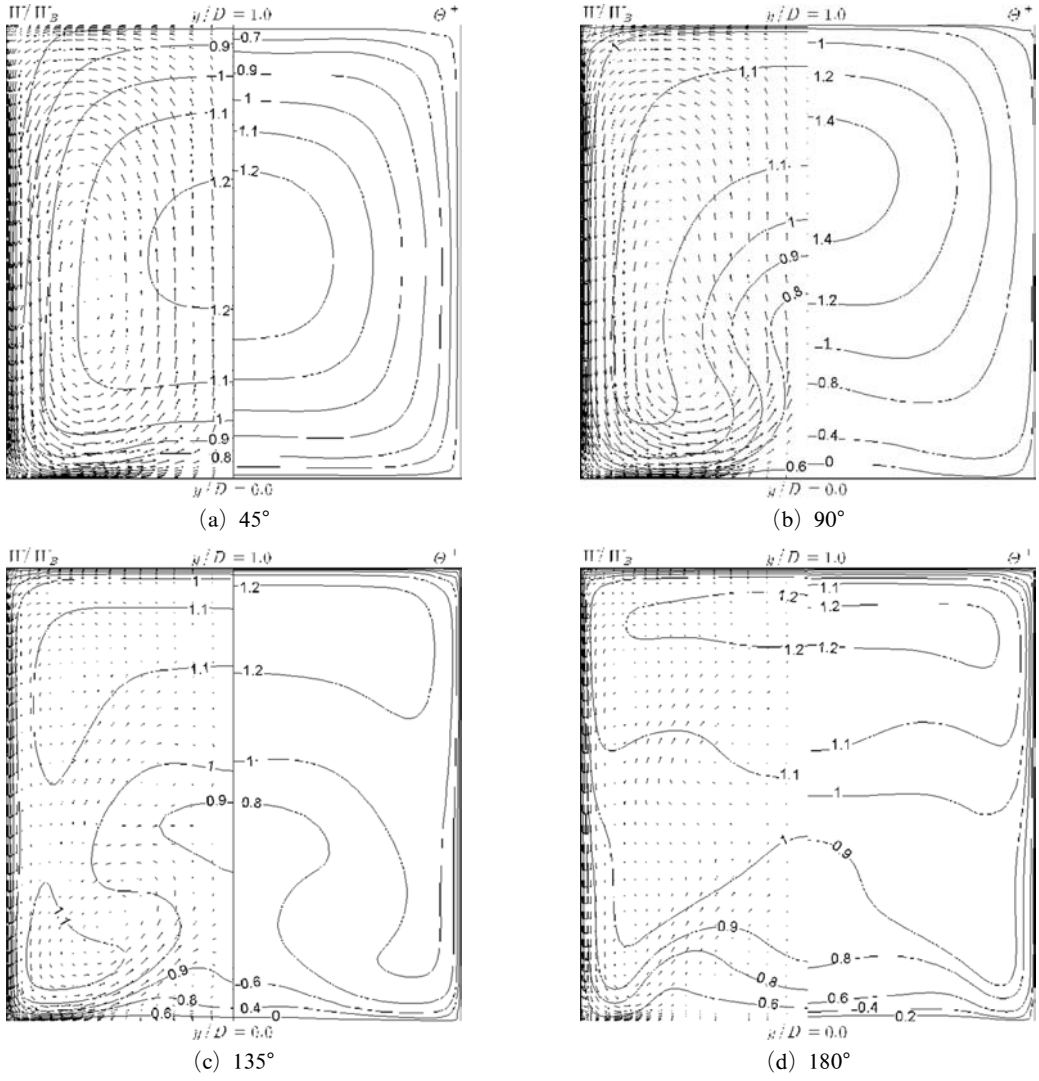

(a) 45° (b) 90°

(c) 135° (d) 180°

Fig. 6 Secondary flow vectors, mean velocity contours and non-dimensional temperature contours in the U-bend duct at Re=56690

the absence of heat transfer along the x direction. Accordingly, the forced convection in square sectioned U-bend duct flow is directly affected by the flow field.

Figure 7 represents the turbulent heat flux contours at the sections of θ=45°, 90°, 135° and 180°, which were predicted by the present EBHM only, and the distributions obtained from the GGDH model, which are not represented in this figure, are very similar to those of EBHM. As shown in the figures, the radial direction turbulent heat flux $\overline{u\theta}$ was symmetrically predicted at the symmetry plane of the cross-section, while the distributions of streamwise heat flux $\overline{u\theta}$ were reproduced to 0 at the symmetry plane. Also, we can infer, from the predicted contour pattern, that the distribution of $\overline{v\theta}$ was much affected by the streamwise velocity and mean temperature profiles.

The results presented in the present article were, overall, in reasonable agreement with the experimental data, giving confidence that the present elliptic concept heat flux model combined with the EBM can be applied to industrial flows with heat transfer. Also, the GGDH model coupled

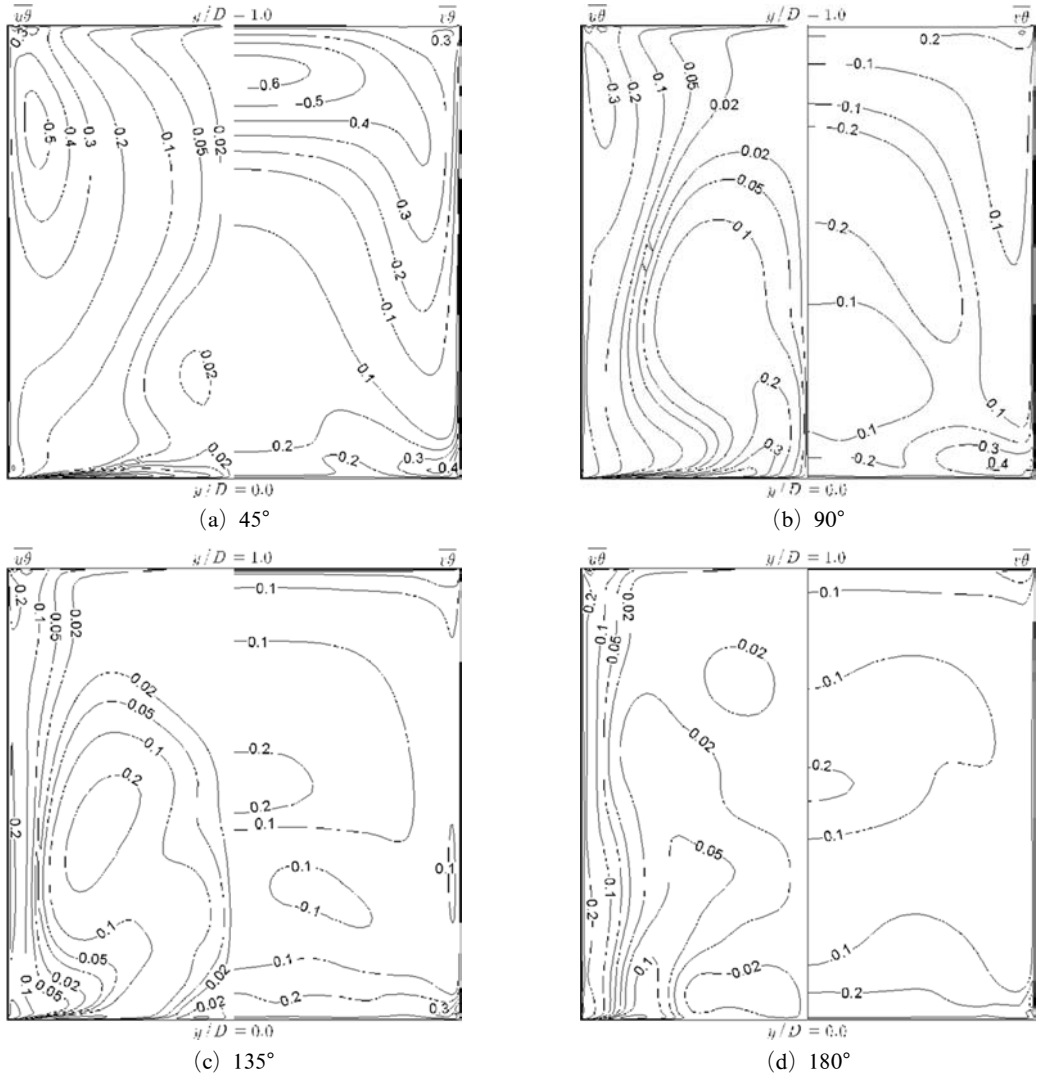

(a) 45° (b) 90°

(c) 135° (d) 180°

Fig. 7 Streamwise and radial direction turbulent heat flux distributions in the U-bend duct at Re=56690

with EBM was appropriately successful for predicting the thermal characteristics in the square sectioned U-bend duct thermal flow, since near-wall turbulence anisotropy was well reproduced by the EBM.

Although the EBHM coupled with EBM solves directly the modelled transport equations which satisfies the limiting wall behaviour of the turbulent heat fluxes, the prediction results are similar to those of the simple GGDH model coupled with EBM. This fact means that the correct resolution of flow field including the Reynolds stresses in the vicinity of the wall is firstly required for the prediction of forced convection heat transfer.

5. Conclusions

The elliptic-blending heat flux model (EBHM), which is closely associated with EBM of Thielen et al., was applied to the square sectioned U-bend duct flow with heat transfer. The appropriateness of the elliptic-blending second moment closure and heat flux model was directly examined by comparing the prediction results with the experimental data. We conclude the following:

(1) The predictions of turbulent flow and heat transfer in the square sectioned U-bend duct by EBHM coupled with EBM, which solves the turbulent heat flux transport equation, were reasonably accurate. Also, despite the simplicity, the GGDH model preserved a proper appropriateness when it was coupled with the EBM. This fact means that the GGDH model can be adopted successfully in complex turbulent heat transfer prediction when near-wall turbulence anisotropy is well reproduced.

(2) The non-dimensional temperature contour pattern was very similar to the streamwise mean velocity contour, except at $\theta=90°$. That is, the non-dimensional temperature distribution was strongly affected by the steamwise velocity. Also, the levels of agreement between the models and experiments for the local Nusselt number distributions were fairly reasonable, though some discrepancies were shown at $\theta=45°$ and 90° of the outer wall. The high level local Nusselt number distributions at $\theta=45°$ and 90° are the consequence of the over-prediction of the non-dimensional temperature profiles in outer wall region.

(3) The distributions of non-dimensional temperature and local Nusselt number by the EBHM coupled with EBM were reasonably well reproduced, when compared to those by the experiments, suggesting that it can be applied to more complex industrial geometries. This result means that the possibility for industrial application can be increased in using the elliptic concept second moment closure.

Acknowledgments

This study was supported by the Korea Science and Engineering Foundation Grant R05-2003-000-12391-0. One of the authors, Y.D. Choi would like to thank for the financial assistance the Korea Science and Engineering Foundation Grant R01-2003-000-10571-0.

References

Chang, S. M., Humphrey, J.A. C. and Modavi, A., 1983, "Turbulent Flow in a Strongly Curved U-Bend and Downstream Tangent of Square Cross-Sections," *Phys. Chem. Hydrodyn.*, Vol. 4, pp. 243～269.

Choi, Y. D., Iacovides, H. and Launder, B. E., 1989, "Numerical Computation of Turbulent Flow in a Square-Sectioned 180 Deg. Bend," *ASME J. of Fluid Engng*, Vol. 111, pp. 59～68.

Craft T. J. and Launder, B. E., 1996, "A Reynolds Stress Closure Designed for Complex Geometries," *Int. J. Heat Fluid Flow*, Vol. 17, pp. 245～254.

Daly, B. J. and Harlow, F. H., 1970, "Transport Equation in Turbulence," *Phys. Fluids*, pp. 2634～2649.

Durbin, P. A., 1993, "A Reynolds Stress Models for Near-wall Turbulence," *J. Fluid Mech.*, Vol. 249, pp. 465～498.

Iacovides, H. and Launder, B. E., 1995, "Computational Fluid Dynamics Applied to Internal Gas-Turbine Blade Cooling : A Review," *Int. J. Heat Fluid Flow*, Vol. 16, pp. 454～470.

Iacovides, H., Launder, B. E. and Li, H. Y., 1996, "Application of a Reflection-Free DSM to Turbulent Flow and Heat Transfer in a Square-Sectioned U-Bend," *Exper. Therm. Fluid Sci.*, Vol. 13, pp. 419～429.

Johnson, R. W., 1984, "Turbulent Convecting Flow in a Square Duct with a 180° Bend ; Experimental and Numerical study," PhD. Thesis, UMIST.

Johnson, R. W. and Launder, B. E., 1985, "Local Nusselt Number and Temperature Field in Turbulent Flow Through a Heated Square-Sectioned U-Bend," *Int. J. Heat Fluid Flow*, Vol. 6, pp. 171～180.

Lai, Y. G. and So, R. M. C., 1990, "Near-Wall Modeling of Turbulent Heat Fluxes," *Int. J. Heat Mass Transfer*, Vol. 33, pp. 1429～1440.

Launder, B. E. 1988, "On the Computation of Convective Heat Transfer in Complex Turbulent Flow," *J. Heat Transfer*, Vol. 110, pp. 1112～1128.

Manceau, R. and Hanjalic, K. 2002, "Elliptic Blending Model : A New Near-Wall Reynolds-Stress Turbulence Closure," *Phys. Fluids*, Vol. 14, pp. 744～754.

Melling, A. and Whitelaw, J. H., 1976, "Tur-

bulence Flow in a Rectangular Duct," *J. Fluid Mech.*, Vol. 78, pp. 289～315.

Shin, J. K., An, J. S. and Choi, Y. D., 2005, "Prediction of Combined Forced and Natural Turbulent Convection in a Vertical Plane Channel with an Elliptic-Blending Second Moment Closure," *Trans. of the KSME* (*B*), Vol. 29, pp. 1265～1276.

Speziale, C. G., Sarkar, S. and Gatski, T. B., 1994, "Modelling the Pressure-Strain Correlation of Turbulence : An Invariant Dynamical System Approach," *J. Fluid Mech.*, Vol. 227, pp. 245～272.

Suga, K. and Abe, K, 2000, "Nonlinear Eddy Viscosity Modelling for Turbulence and Heat Transfer Near Wall and Shear-Free Boundaries," *Int. J. Heat Mass Transfer*, Vol. 21, pp. 37～48.

Suga, K., 2003, "Predicting Turbulence and Heat Transfer in 3-D Curved Ducts by Near-Wall Second Moment Closures," *Int. J. Heat Mass Transfer*, Vol. 46, pp. 161～173.

Thielen, L., Hanjalic, K., Jonker, H. and Manceau, R., 2004, "Prediction of Flow and Heat Transfer in Multiple Impinging Jets with an Elliptic-Blending Second-Moment Closure," *Int. J. Heat Mass Transfer*, Vol. 48, pp. 1583～1598.